

# Dynamic study on fusion reactions for $^{40,48}\text{Ca} + ^{90,96}\text{Zr}$ around Coulomb barrier \*

Ning Wang<sup>1,\*</sup>, Xizhen Wu<sup>1,2,†</sup>, Zhuxia Li<sup>1,2,3,†</sup>

1) *China Institute of Atomic Energy, P. O. Box 275(18),*

*Beijing 102413, People Republic of China*

2) *Nuclear Theory Center of National Laboratory of Heavy Ion Accelerator,*

*Lanzhou 730000, People Republic of China*

3) *Institute of Theoretical Physics, Chinese Academy of Sciences,*

*Beijing 100080, People Republic of China*

## Abstract

By using the updated improved Quantum Molecular Dynamics model in which a surface-symmetry potential term has been introduced for the first time, the excitation functions for fusion reactions of  $^{40,48}\text{Ca} + ^{90,96}\text{Zr}$  at energies around the Coulomb barrier have been studied. The experimental data of the fusion cross sections for  $^{40}\text{Ca} + ^{90,96}\text{Zr}$  have been reproduced remarkably well without introducing any new parameters. The fusion cross sections for the neutron-rich fusion reactions of  $^{48}\text{Ca} + ^{90,96}\text{Zr}$  around the Coulomb barrier are predicted to be enhanced compared with a non-neutron-rich fusion reaction. In order to clarify the mechanism of the enhancement of the fusion cross sections for neutron-rich nuclear fusions, we pay a great attention to study the dynamic lowering of the Coulomb barrier during a neck formation. The isospin effect on the barrier lowering is investigated. It is interesting that the

---

\*\*Email address: wangning@iris.ciae.ac.cn

†Email address: lizwux@iris.ciae.ac.cn

effect of the projectile and target nuclear structure on fusion dynamics can be revealed to a certain extent in our approach. The time evolution of the N/Z ratio at the neck region has been firstly illustrated. A large enhancement of the N/Z ratio at neck region for neutron-rich nuclear fusion reactions is found.

PACS numbers: 25.70.-z, 24.10.-i

## 1. INTRODUCTION

Being encouraged by the synthesis of superheavy elements, the investigation on fusion mechanism at low energies has recently received a great attention both theoretically and experimentally [1–8]. Since the central region of superheavy elements were predicted to locate at  $Z=114$  or 120 and  $N=184$ , which is strongly neutron-rich, the study of dynamics for neutron-rich fusion reactions is highly demanded for the purpose of the synthesis of superheavy elements. The dynamics of fusion process for normal nuclear systems has been studied in [9–15]. In these studies, it has been shown that the neck formation, dynamical deformation, etc, result in a lowering of the fusion barrier and furthermore it has been demonstrated that this lowering effect is mostly significant at energies near the barrier, consequently the sub-barrier fusion cross sections are enhanced compared with the prediction of WKB approximation. But for neutron-rich systems, the dynamics of fusion process is much less studied. For neutron-rich systems, the symmetry term of EOS should play a significant dynamical role. Therefore it seems to us that it is highly requisite to study how the symmetry potential influences the mechanism of neutron-rich fusion reaction process dynamically. In this work, we devote ourselves to study the fusion dynamics for neutron-rich systems at energies around the barrier by means of the improved quantum molecular dynamics (ImQMD) model [16]. In ref. [16] we have shown that the ImQMD model can describe the properties of the ground state of selected nuclei from  $^6Li$  to  $^{208}Pb$  very well with one set of parameters and the experimental data of fusion reaction cross sections for  $^{40}Ca+^{90,96}Zr$  [7] can also be reproduced well with no extra-parameters. From that study,

the experimentally observed enhancement of fusion cross sections for  $^{40}\text{Ca}+^{96}\text{Zr}$  compared with the non-neutron-rich fusion reaction of  $^{40}\text{Ca}+^{90}\text{Zr}$  was attributed to gaining a stronger dynamical lowering effect of the Coulomb barrier for the neutron-rich target reaction of  $^{40}\text{Ca}+^{96}\text{Zr}$ . Based on that investigation, it would be very interesting to study the dynamics of fusion reactions induced by the neutron-rich projectile  $^{48}\text{Ca}$  at energies around the Coulomb barrier with the same model. As is well known that  $^{48}\text{Ca}$  has double closed shell structure and spherical shape as the same as  $^{40}\text{Ca}$ . Therefore, the static deformation effect of the projectile on the enhancement of fusion cross sections at energies around the barrier can be ruled out, and the role of the isospin effect should be shown up by a comparison between two cases. But, on the other hand, the shell structure of  $^{48}\text{Ca}$  is rather different from  $^{40}\text{Ca}$  and the energy of octupole vibrations of  $^{48}\text{Ca}$  is about 1 MeV higher than that of  $^{40}\text{Ca}$  due to the shell structure. Furthermore, from the inelastic scattering study it has been shown that  $^{40}\text{Ca}$  has a stronger octupole vibration than  $^{48}\text{Ca}$  [6]. The situation is different for Zr isotopes for which the energy of  $3^-$  state decreases as the number of neutrons increases from  $^{90}\text{Zr}$  to  $^{96}\text{Zr}$ . This structure effect should influence the fusion dynamics and the fusion cross sections as well. It is not clear how to explicitly implement this effect into our model at this moment. However, a dynamical study on the neutron-rich fusion reactions can provide us with the information about dynamical deformation which may relate to the structure of projectile and target in addition to the information of isospin effect on a fusion process, which are quite general. In this work, we make comparison of the dynamic barrier lowering effect for 4 reaction systems  $^{40,48}\text{Ca}+^{90,96}\text{Zr}$  at energies around the barrier, and furthermore we analyze the causes for the dynamic barrier lowering in detail, mainly focus on the stage of the neck formation and neck development.

The paper is organized as follows: In sec. II we briefly introduce our ImQMD model. Then we study the mechanism of neutron-rich nuclear fusion reactions in sec. III. Finally, a short summary and discussion are given in sec IV.

## II. IMPROVED QMD MODEL

For reader convenience, in this section we briefly introduce the ImQMD model. In the ImQMD model as the same as in the original QMD model [17–20], each nucleon is represented by a coherent state of a Gaussian wave packet

$$\phi_i(\mathbf{r}) = \frac{1}{(2\pi\sigma_r^2)^{3/4}} \exp\left[-\frac{(\mathbf{r} - \mathbf{r}_i)^2}{4\sigma_r^2} + \frac{i}{\hbar} \mathbf{r} \cdot \mathbf{p}_i\right], \quad (1)$$

where  $\mathbf{r}_i$  and  $\mathbf{p}_i$  are the centers of the  $i$ -th wave packet in the coordinate and momentum space, respectively.  $\sigma_r$  represents the spatial spread of the wave packet. Through a Wigner transformation of the wave function, the one-body phase space distribution function for  $N$ -distinguishable particles is given by:

$$f(\mathbf{r}, \mathbf{p}) = \sum_i f_i(\mathbf{r}, \mathbf{p}). \quad (2)$$

where

$$f_i(\mathbf{r}, \mathbf{p}) = \frac{1}{(\pi\hbar)^3} \exp\left[-\frac{(\mathbf{r} - \mathbf{r}_i)^2}{2\sigma_r^2} - \frac{2\sigma_r^2}{\hbar^2}(\mathbf{p} - \mathbf{p}_i)^2\right]. \quad (3)$$

For identical Fermions, the effects of the Pauli principle are discussed in a broader context by Feldmeier and Schnack [21]. The approximative treatment of anti-symmetrisation used in this paper is explained below. The density and momentum distribution function of a system read

$$\rho(\mathbf{r}) = \int f(\mathbf{r}, \mathbf{p}) d^3p = \sum_i \rho_i(\mathbf{r}), \quad (4)$$

$$g(\mathbf{p}) = \int f(\mathbf{r}, \mathbf{p}) d^3r = \sum_i g_i(\mathbf{p}), \quad (5)$$

respectively, where the sum runs over all particles in the system.  $\rho_i(\mathbf{r})$  and  $g_i(\mathbf{p})$  are the density and momentum distribution function of nucleon  $i$ :

$$\rho_i(\mathbf{r}) = \frac{1}{(2\pi\sigma_r^2)^{3/2}} \exp\left[-\frac{(\mathbf{r} - \mathbf{r}_i)^2}{2\sigma_r^2}\right], \quad (6)$$

$$g_i(\mathbf{p}) = \frac{1}{(2\pi\sigma_p^2)^{3/2}} \exp\left[-\frac{(\mathbf{p} - \mathbf{p}_i)^2}{2\sigma_p^2}\right], \quad (7)$$

where  $\sigma_r$  and  $\sigma_p$  are the widths of wave packets in coordinate and momentum space, respectively, and they satisfy the minimum uncertainty relation. The time evolution of  $\mathbf{r}_i$  and  $\mathbf{p}_i$  is governed by Hamiltonian equations of motion:

$$\dot{\mathbf{r}}_i = \frac{\partial H}{\partial \mathbf{p}_i}, \dot{\mathbf{p}}_i = -\frac{\partial H}{\partial \mathbf{r}_i}. \quad (8)$$

The Hamiltonian  $H$  consists of the kinetic energy and the effective interaction potential energy:

$$H = T + U. \quad (9)$$

The effective interaction potential energy includes the nuclear local interaction potential energy and Coulomb interaction potential energy:

$$U = U_{loc} + U_{coul}, \quad (10)$$

and

$$U_{loc} = \int V_{loc} d^3 \mathbf{r}. \quad (11)$$

$V_{loc}$  is the potential energy density, which can be derived directly from a zero-range Skyrme interaction [23,24]. Thus,

$$U_{loc} = \frac{\alpha}{2} \sum_i \langle \frac{\rho}{\rho_0} \rangle_i + \frac{\beta}{3} \sum_i \langle \frac{\rho}{\rho_0} \rangle_i^2 + \frac{C_s}{2} \int \frac{(\rho_p - \rho_n)^2}{\rho_0} d^3 \mathbf{r} + \int \frac{g_1}{2} (\nabla \rho)^2 d^3 \mathbf{r}, \quad (12)$$

where

$$\langle \rho \rangle_i = \sum_{j \neq i} \rho_{ij}, \quad (13)$$

and

$$\rho_{ij} = \frac{1}{(4\pi\sigma_r^2)^{3/2}} \exp\left[-\frac{(\mathbf{r}_i - \mathbf{r}_j)^2}{4\sigma_r^2}\right]. \quad (14)$$

The third term in the right hand side of (12) is the symmetry potential energy. The gradient term in  $U_{loc}$  is to account for the surface energy and the correction to the second term in Equ.(12) [16,23].

Because in this work we are going to study the isospin effect on the fusion dynamics in neutron-rich nuclear fusion reactions we pay a special attention to the symmetry potential term. Therefore we make a more careful treatment on the symmetry potential term, namely, in addition to the volume symmetry potential term, we further introduce a surface symmetry potential term according to the finite-range Liquid-Drop Model [25], which reads as

$$U_{sur-sym} = \frac{C_s C_k}{2\rho_0} \sum_{i,j \neq i} s_i s_j \rho_{ij} \nabla_i^2 \rho_{ij}. \quad (15)$$

Where,  $s_i$  is +1 for proton and -1 for neutron and  $C_k$  is the strength parameter for the surface symmetry term. We find this term plays an important dynamical role for reactions  $^{48}\text{Ca} + ^{90,96}\text{Zr}$  but a minor role for  $^{40}\text{Ca} + ^{90,96}\text{Zr}$ . It reduces the fusion cross sections for  $^{48}\text{Ca} + ^{90,96}\text{Zr}$  considerably but almost does not change the cross sections of  $^{40}\text{Ca} + ^{90,96}\text{Zr}$ . The discussion about the effect of this term will be given elsewhere. The parameters used in this work are listed in Table I

Considering the fact that for a finite system the nucleons are localized in a finite region corresponding to the size of the system, the width of wave packets representing nucleons in the system should have a relation with the size of the system. As the same as in [16], here we also adopt a system size dependent wave packet width to account for the fact, that is,

$$\sigma_r = 0.16N^{1/3} + 0.49, \quad (16)$$

where  $N$  is the number of nucleons bound in the system.

In order to overcome the difficulty in describing the Fermionic nature of N-body system in the QMD model, an approximative treatment of antisymmetrization is adopted, namely, we implement the phase space constraint of the CoMD model proposed by Papa.et.al. [26] into the model. It is requested by the constraint that the one body occupation number in a volume  $h^3$  of phase space centered at  $(\mathbf{r}_i, \mathbf{p}_i)$  corresponding to the centroid of wave packet of particle i should always be not larger than 1 according to the Pauli principle. The one body occupation number is calculated by

$$f_i^{ocu} = \sum_j \delta_{\tau_i \tau_j} \delta_{s_i s_j} \int_{h^3} f_j(\mathbf{r}, \mathbf{p}) d^3 \mathbf{r} d^3 \mathbf{p}, \quad (17)$$

where  $s_i$  and  $\tau_i$  are the third component of spin and isospin of particle  $i$ . We have made a check for time evolution of individual nuclei from light nuclei to heavy nuclei and we found that by taking the procedure of phase space constraint, the requirement is reasonably satisfied and the phase space distribution is prevented efficiently from evolving to be a classical distribution from the initial nuclear ground state distribution for a long enough time.

Concerning the collision part, an isospin dependent nucleon-nucleon scattering cross section and Pauli-blocking are used [27,11]. This part actually plays a minor role in a fusion reaction.

In this work the initial density distribution of projectile and target is obtained by Skyrme HF calculations [28,29]. The other procedures are the same as in [16]. The model has been carefully checked and it turns out that the ImQMD model works well in describing the ground state properties for nuclei from  $^6\text{Li}$  to  $^{208}\text{Pb}$  and calculating the static Coulomb barrier for fusion reactions as well as fusion cross sections for  $^{40}\text{Ca}+^{90,96}\text{Zr}$ .

### 3. RESULTS

Before coming to the numerical results for fusion reactions  $^{40,48}\text{Ca}+^{90,96}\text{Zr}$ , let us first make a survey on the configurations along a fusion path. In Fig.1 we illustrate one typical fusion event of the head on reaction of  $^{40}\text{Ca}+^{90}\text{Zr}$  at the energy 5 MeV below the barrier. In the figure, we plot the dynamical barrier  $V_b$  as a function of the distance between the center of mass of projectile and that of target. We will discuss the dynamical barrier in more detail in the following section (section B) and the definition of it will be given there. Simultaneously in sub-figures we plot the contour plots of density distributions as well as the corresponding single-particle potentials at 3 typical time, i.e. before, at, and after reaching the highest value of the dynamic barrier along the fusion path. The single-particle potential is calculated by

$$V_{sp}(\mathbf{r}) = \int \rho(\mathbf{r}') V(\mathbf{r} - \mathbf{r}') d^3\mathbf{r}', \quad (18)$$

with  $\rho(\mathbf{r})$  being the density distribution of the system and  $V(\mathbf{r} - \mathbf{r}')$  the effective nucleon-nucleon interaction. In sub-figures(1a)and (1b) we plot the contour plot of the density distribution as well as the corresponding single-particle potential at the point 1 along the fusion path. One can find from these two sub-figures that at this point the fusion partners are not in touch( see sub-figure (1a)) and there is a high enough inner potential barrier which prevents nucleons moving from the projectile to target or vice versa ( see sub-figure(1b)). At the time corresponding to the point 2, the dynamic barrier reaches a maximum value. The contour plot of density distribution( sub-figure(2a)) shows that the fusion partners are at the touching configuration and a neck starts to grow and following it, the inner potential barrier in the potential well is reduced allowing a few nucleons moving from projectile to target or vice versa(see sub-figure(2b)). At the time corresponding to the point 3, the dynamical barrier is reduced considerably. Sub-fig.(3a) and sub-fig.(3b) show that the neck develops considerably at this time and consequently, the inner potential barrier in the potential well is reduced substantially and nucleon transfer between the projectile and target becomes much easier than before. This means that a pre-compound nucleus begins to be formed. From this study we have learned that how the dynamical fusion barrier is correlated with the development of the configuration of fusion partners along the fusion path.

In the following, we show the numerical results for fusion reactions  $^{40,48}\text{Ca} + ^{90,96}\text{Zr}$ . First we show the fusion cross sections. For understanding the mechanism of the enhancement of the fusion cross sections for  $^{40}\text{Ca} + ^{96}\text{Zr}$  and  $^{48}\text{Ca} + ^{90,96}\text{Zr}$  compared with  $^{40}\text{Ca} + ^{90}\text{Zr}$  case, we show the dynamic barrier and the other quantities relevant to the dynamic lowering of the Coulomb barrier only at head on reactions. Following it we make a discussion about the isospin and structure effect in fusion dynamics for the systems studied. In order to exploring how the isospin transfers at the neck region, we study the time evolution of the N/Z ratio at the neck region for  $^{40,48}\text{Ca} + ^{90,96}\text{Zr}$  reactions to see how it depends on the initial N/Z ratio.

## A. FUSION CROSS SECTIONS FOR $^{40,48}\text{Ca} + ^{90,96}\text{Zr}$

After making the preparation of initial nuclei, we elaborately select ten projectile nuclei and ten target nuclei from thousands of pre-prepared systems. By rotating these prepared

projectile and target nuclei around their centers of mass by a Euler angle chosen randomly, we create 100 bombarding events for each reaction energy  $E$  and impact parameter  $b$ . Through counting the number of fusion events, we obtain the probability of fusion reaction  $g_{fus}(E, b)$ , then the cross section is calculated by using the expression:

$$\sigma_{fus} = 2\pi \int_0^{b_{\max}} b g_{fus}(E, b) db = 2\pi \sum b g_{fus}(E, b) \Delta b. \quad (19)$$

The distance from projectile to target at initial time is taken to be 20 fm.

As for the definition of fusion event, we still adopt an operational definition as the same as in TDHF calculations and in the QMD model calculations [31]. More specifically, in this work we consider any event, for which the number of nucleons escaped during the process of forming compound nuclei is equal to or less than 6, as a fusion event [16]. Fig.2 shows the fusion cross sections for  $^{40}\text{Ca}+^{90}\text{Zr}$ ,  $^{40}\text{Ca}+^{96}\text{Zr}$ ,  $^{40}\text{Ca}+^{90}\text{Zr}$ , and  $^{40}\text{Ca}+^{90}\text{Zr}$ , respectively. Experimental data for the reactions of  $^{40}\text{Ca}+^{90,96}\text{Zr}$  taken from ref. [7] are also shown. One can see that the experimental data for  $^{40}\text{Ca}+^{90,96}\text{Zr}$  are reproduced well without introducing new parameters and there is a strong enhancement of the fusion cross sections for neutron-rich reactions. The fusion cross sections for reactions  $^{48}\text{Ca}+^{90,96}\text{Zr}$  at energies around the barrier are higher than those for  $^{40}\text{Ca}+^{96}\text{Zr}$ . But the enhancement of the fusion cross sections for  $^{48}\text{Ca}+^{90,96}\text{Zr}$  compared with  $^{40}\text{Ca}+^{96}\text{Zr}$  is not so strong as the case of  $^{40}\text{Ca}+^{96}\text{Zr}$  compared with  $^{40}\text{Ca}+^{90}\text{Zr}$ . For understanding the feature of the fusion excitation functions for different systems shown in Fig.2, let us first look at the distribution of fusion probabilities with respect to the impact parameters in Fig.3. One can find in the figure that for neutron-rich reactions, in addition to having a larger fusion probability, the maximum impact parameter leading to fusion is larger compared with non-neutron-rich reactions. For example, at the incident energy 5 MeV below the static Coulomb barrier, the maximum impact parameter leading to fusion is about 9 fm for reaction  $^{48}\text{Ca}+^{90,96}\text{Zr}$ , about 8.5 fm for  $^{40}\text{Ca}+^{96}\text{Zr}$ , and only 6.5 fm for the non-neutron-rich reaction of  $^{40}\text{Ca}+^{90}\text{Zr}$ . This means that for the neutron-rich reactions, the fusion partners can be fused at a relative larger distance. A possible reason for it is that the dynamical elongation is enhanced for neutron-rich fusion systems. The effect

of the dynamical elongation on dynamical lowering of the Coulomb barrier will be discussed in the following section.

For the cases of the incident energy at 10 MeV above the static Coulomb barrier, the distribution of the fusion probability with respect to the impact parameter shows a similar tendency but the effect is weaker.

## B. DYNAMIC LOWERING OF THE BARRIER

In order to understand the reason for the enhancement of fusion reaction cross sections for neutron-rich nuclear fusions in this section we study the dynamic Coulomb barrier lowering effect. In the QMD model, the Coulomb barrier is calculated microscopically by using the following expressions

$$V_b(d) = \int d^3r_1 \int d^3r_2 \rho_1(\mathbf{r}_1 - \mathbf{r}_{1c}) V(\mathbf{r}_1 - \mathbf{r}_2) \rho_2(\mathbf{r}_2 - \mathbf{r}_{2c}), \quad (20)$$

$$d = |\mathbf{r}_{1c} - \mathbf{r}_{2c}|,$$

where  $\rho_1$ ,  $\rho_2$  are the density distribution of projectile and target, respectively;  $\mathbf{r}_{1c}$ ,  $\mathbf{r}_{2c}$  are their centers of mass, respectively.  $V(\mathbf{r} - \mathbf{r}')$  is the effective nucleon-nucleon interaction. It is clear that, in general,  $V_b(d)$  is a function of time since  $\rho_1$ ,  $\rho_2$  changes from time to time. Only in a static case, where the density distribution of projectile and target assumes to be the same as that at the initial time and correspondingly the static barrier is calculated with the static density distribution. Therefore for the static barrier, the dynamical effects experienced by fusion partners during reaction process are not taken into account. For dynamic case, the density distribution of the projectile and target is calculated by using expression(4) with sum running over all particles in projectile and target, respectively. When two colliding partners approach with each other, the density distribution of projectile and target changes from time to time and their shape (determined by the density distribution) get deformed due to the interaction between them. The time evolution of the shape deformation and the neck formation depends on the incident system and energy as well as the impact parameter. Consequently, the dynamical barrier not only depends on the incident system but also depends on the incident energy as well as the impact parameter. In the following we

only study the head on collision case and define the height of the highest Coulomb barrier experienced in the path of fusion as the height of the dynamic Coulomb barrier.

Generally, the dynamic barrier is lower than that of the static one because of the neck formation and the increase of the N/Z ratio at neck region for neutron-rich nuclear fusion reactions. As an example, in table II we show the results about the dynamic barrier for head on fusion reactions of  $^{40,48}\text{Ca} + ^{90,96}\text{Zr}$  at energies 5 MeV below and 10 MeV above the static Coulomb barrier. From this table one can see that the dynamic effect lowers the height of barrier dramatically and this dynamic lowering is incident energy and system dependent. The barrier lowering is stronger for the case of the energy below the barrier than that of the energy above the barrier. This feature of barrier lowering was also observed in [15] for symmetric reactions of oxygen and nickel isotopes by means of the mean field transport theory.

To illustrate the system dependence of the dynamic barrier, in Fig.4 we show the time evolution of the dynamic barrier for head on collisions of  $^{40,48}\text{Ca} + ^{90,96}\text{Zr}$  at the incident energy 5 MeV below the static barrier. From a comparison among four curves we see the following trends: 1) The dynamic Coulomb barrier for neutron-rich reactions is lower than that for non-neutron-rich reactions. 2) The barrier top position for neutron-rich reactions is shifted to a larger distance compared to non-neutron-rich ones. 3) The width of the barrier for neutron-rich reactions is thinner than that for non-neutron-rich reactions. As for three neutron-rich reactions, there is no obvious difference in the dynamic Coulomb barrier.

To investigate the causes leading to these trends let's turn to study the quantities relevant to the dynamic barrier. For the purpose of understanding the mechanism, in Table III we only give the calculation results for head on collisions of  $^{40,48}\text{Ca} + ^{90,96}\text{Zr}$  at energies of 5 MeV below (lower energy case) and 10 MeV above (higher energy case) the corresponding static Coulomb barrier. The quantities listed in table III are calculated as follows: for each event, we calculate the  $V_b(d)$  at each time step to find out the time of reaching the highest barrier (i.e. the point 2 in Fig. 1). The contour map with  $\rho = 0.02/fm^3$  of the density distribution of the system at this time gives the shape of the system (see sub-figure(2a) of Fig.1). The

schematic figure of Fig.5 illustrates the shape of the system (typically for a head on collision) at this time and the geometry quantities listed in table III, such as the distance between the centers of mass of projectile and target, and the neck radius,etc, are shown in the figure. The results given in Table III are the average values of all corresponding events. The elongation given in table III equals the distance between the centers of mass of projectile and target minus the radii of initial projectile and target nuclei. From Table III one can find that the height of the dynamic barrier is closely correlated with the elongations obtained for different incident energies and collision systems listed in the table , i.e. the larger the elongation is the lower the barrier is. Generally speaking, the elongation at the touching configuration should depend on the interaction time before reaching the touching configuration and the longer interaction time leads to a larger elongation. Therefore the elongation for the lower energy case is always larger than that for the higher energy case. Table III shows that the elongation for energy below static barrier case is about 10 % larger than that for above static barrier case. Furthermore, the elongation also depend on structure of projectile and target and the N/Z ratio at neck region as well. Now let's look at the dependence of the elongation on the structure of reaction systems. For the lower energy case, the largest elongation is obtained in the reaction of  $^{40}\text{Ca}+^{96}\text{Zr}$ , while for the higher energy case the largest elongation is obtained in  $^{48}\text{Ca}+^{96}\text{Zr}$ . As is well known that the energy of octupole vibration of  $^{96}\text{Zr}$  is lower than that of  $^{90}\text{Zr}$  and we may consider  $^{96}\text{Zr}$  is softer than  $^{90}\text{Zr}$ . And for  $^{48}\text{Ca}$ , the energy of octupole vibration is about one MeV higher than that of  $^{40}\text{Ca}$  , which implies that  $^{48}\text{Ca}$  is more rigid than  $^{40}\text{Ca}$ . The dependence of the elongation on the different systems given in Table III clearly shows the influence of nuclear structure effect. Concerning the isospin effect, it is quite natural that the increase of N/Z at neck region should decrease the height of the Coulomb barrier. There is a strong enhancement of the N/Z ratio at neck region for neutron-rich reactions as shown in Table III. Consequently, for  $^{40}\text{Ca}+^{96}\text{Zr}$  compared with  $^{40}\text{Ca}+^{90}\text{Zr}$  both the isospin effect and the structure effect are in favor to enhance the fusion cross sections of  $^{40}\text{Ca}+^{96}\text{Zr}$ . While for reactions induced by  $^{48}\text{Ca}$  compared with reactions induced by  $^{40}\text{Ca}$ , the isospin effect and the structure effect are counterpart, consequently

the enhancement of fusion cross section induced by neutron-rich effect is reduced by the structure effect.

### C. TIME EVOLUTION OF THE N/Z RATIO AT THE NECK REGION

As is seen from above study that the dynamic lowering of the barrier is closely related to the configuration and component of the neck. The N/Z ratio at the neck region is one of the most sensitive quantities with respect to the neck formation for neutron-rich nuclear fusion reactions, as shown in table III. For the isospin symmetry case of  $^{40}\text{Ca} + ^{90}\text{Zr}$ , the N/Z ratio at the neck region is more or less the same as the average N/Z ratio of the total system. But for the neutron-rich reactions, the N/Z ratio at the neck region is much higher than that of the average N/Z value of the corresponding systems. This effect results from the different behavior of the density dependence of chemical potential for neutrons and protons in isospin asymmetry systems. The chemical potential is defined as

$$\mu_{n/p} = \frac{\partial \varepsilon(\rho, \delta)}{\partial \rho_{n/p}}, \quad (21)$$

where  $\varepsilon(\rho, \delta)$  is the energy density and  $\mu_{n/p}$  and  $\rho_{n/p}$  are the chemical potential and the density of neutrons and protons, respectively. From the definition one can find that the chemical potential is a function of both density  $\rho$  and isospin asymmetry  $\delta$ . Fig.6 shows the chemical potential of proton and neutron as function of density with  $\delta = \frac{N-Z}{N+Z} = 0.10$ . From Fig.6 one can see that the density corresponding to the minimum of the chemical potential of neutrons is lower than that of protons for a neutron-rich nuclear system and thus the neutrons are preferably driven to the lower density area. This effect has also been studied and confirmed in the intermediate energy heavy ion collisions. The increasing of the N/Z ratio at the neck region should reduce the dynamic barrier in fusion process. It would be interesting to study the isospin transfer at neck region, therefore in Fig.7 we show the time evolution of the N/Z ratio at the neck region for head on fusion reactions of  $^{40,48}\text{Ca} + ^{90,96}\text{Zr}$  at energies 5 MeV below and 10 MeV above the static Coulomb barrier, in which the time is started from the beginning of neck formation (when the density at the touching point reaches  $0.02 \rho_0$ ). The general trend of the time evolution of the N/Z ratio is: the N/Z ratio at the

neck region first increases as time increases, then soon reaches a maximum value and then decreases, finally it approaches the average N/Z value of the system. The figure shows that the enhancement of N/Z at neck region at the early stage of the neck formation strongly depends on the N/Z ratio of the initial system, i.e. the larger the isospin asymmetry of the initial system is, the stronger the enhancement of N/Z ratio at neck region is. The reason for the fluctuation appeared in the time evolution of the N/Z ratio for neutron-rich reactions may be understood as: at the beginning when the neck is just formed, neutrons are preferably move to the neck region driven by the chemical potential; not soon as too many neutrons are concentrated there, the symmetry potential attracts more protons to migrate into the neck region and the N/Z ratio is reduced, and then because of the increase of proton number the Coulomb repulsion plays a role.... Thus the interplay of the Coulomb force and the symmetry potential results in the fluctuation behavior in time evolution of the N/Z ratio at neck region for neutron-rich systems. This fluctuation becomes stronger for non-central collisions. With the growing of neck, nucleon transfer through the neck becomes easier and the fusion system passes over the dynamic barrier. After about 100 fm/c, that is, when a neck develops well, the N/Z ratio at the neck region gradually approaches to the average N/Z ratio of the whole system and the isospin degree of freedom seems to gradually reach an equilibrium, but the dissipation of the collective motion is still going on. The details of the nucleon transfer and the dissipation of the collective motion in the neck region will be discussed elsewhere.

## SUMMARY AND DISCUSSION

In this work we have introduced a surface-symmetry potential term into a QMD type transport model for the first time. We have used this newly updated ImQMD model to study the fusion dynamics of  $^{40,48}\text{Ca} + ^{90,96}\text{Zr}$  at energies around the barrier. The surface-symmetry term seems to play an important role in fusion dynamics for  $^{48}\text{Ca} + ^{90,96}\text{Zr}$  but negligible role in that of  $^{40}\text{Ca} + ^{90,96}\text{Zr}$ . Our calculated results of excitation functions for fusion reactions of  $^{40,48}\text{Ca} + ^{90,96}\text{Zr}$  show a strong enhancement of fusion cross sections for the neutron-rich

reactions at energies near and below the static barrier. We have made systematic analysis to understand this feature. We have shown that the maximum impact parameter leading to fusion reaction for neutron-rich reactions is larger than that for non-neutron-rich reactions, which means that the excess neutrons make the reaction partners to be fused at longer distance.

We have paid a great attention to study the dynamical fusion barrier and found that there is a substantially lowering of the dynamic barrier compared with the static Coulomb barrier due to the neck formation. For the reactions studied we have observed that: 1) The dynamic Coulomb barrier for a neutron-rich configuration is lower than that for a non-neutron-rich case; 2) The barrier top position for a neutron-rich configuration is shifted to a larger distance compared to a non-neutron-rich configuration; 3) The width of the barrier for a neutron-rich configuration is thinner than that for a non-neutron-rich case.

We have shown that the time evolution of the ratio of neutrons to protons ( the N/Z ratio ) at the neck region strongly depends on the projectile and target isospin. At the early stage of the neck formation, the N/Z ratio at neck region can reach a value of twice the average N/Z ratio value of the whole system for  $^{48}\text{Ca}+^{90,96}\text{Zr}$ , then after 100 fm/c later the N/Z ratio at the neck region gradually approaches the average value of the whole system, which means that the isospin degree of freedom gradually approaches an equilibrium before the dissipation of collective motion is completed.

A strong enhancement of fusion cross sections for  $^{40}\text{Ca}+^{96}\text{Zr}$  compared to  $^{40}\text{Ca}+^{90}\text{Zr}$  have been found which is in good agreement with the observation in experiments. Relatively, the enhancement of fusion cross sections for  $^{48}\text{Ca}+^{90,96}\text{Zr}$  compared with  $^{40}\text{Ca}+^{96}\text{Zr}$  is less strong. The dynamic barrier lowering have been studied systematically. We find it strongly relate to the elongation of systems and the N/Z ratio at neck region at the touching configuration on the fusion path. The results seem to show that the elongation at touching configuration for different reaction systems is correlated with the structure of projectile and target. For instance, the largest elongation is obtained in the case of  $^{40}\text{Ca}+^{96}\text{Zr}$  at 5 MeV below the static barrier in consistent with the fact that the energy of octupole vibration decreases from

$^{90}\text{Zr}$  to  $^{96}\text{Zr}$  and from  $^{48}\text{Ca}$  to  $^{40}\text{Ca}$  as well. On the other hand, the isospin effect which strongly influences the N/Z ratio at neck region for neutron-rich nuclear fusion should affect the dynamic barrier strongly and consequently, affect the fusion cross sections of neutron-rich nuclear reactions. Further work on exploring how the isospin effect and structure effect competes in fusion reactions is needed. We strongly urge to make measurements of fusion cross section and the distribution of barrier for  $^{40,48}\text{Ca} + ^{90,96}\text{Zr}$  to explore the interplay between these two effects in fusion reactions.

The problem concerning the mass transfer is not discussed yet and the neck dynamics is still not discussed thoroughly in this paper. The work about these aspects is in progress.

## ACKNOWLEDGMENTS

We thank Profs. H.Q.Zhang and Z.H.Liu for stimulating discussions. The work is supported by the National Natural Science Foundation of China under Grant Nos. 19975073, 10175093, and 10175089, and by the Science Foundation of Chinese Nuclear Industry and Major State Basic Research Development Program under Contract No. G20000774.

## REFERENCES

- [1] V. I. Zagrebaev, Phys. Rev. **C64**, 034606 (2001).
- [2] A. Diaz-Torres, G. G. Adamian, N. V. Antonenko, W. Scheid, Phys. Lett. **B 481**, 228 (2000).
- [3] G. G. Adamian, N. V. Antonenko, A. Diaz-Torres, W. Scheid. Nucl. Phys. **A 671**, 233 (2000).
- [4] Toshiki Maruyama, A. Bonasera, Massimo Papa, S. Chiba, nucl-th/0107021.
- [5] Y. Aritomo, T. Wada, M. Ohta and Y. Abe, in proceedings on Fusion dynamics at the extremes, Dubna, 2000, edited by Yu. Oganessian and V. Zagrebaev ( world Scientific, Singapore 2001) P. 123;  
Y. Abe, C. W. Shen and G. Kosenko, in AIP conference proceedings 597 on Nonequilibrium and nonlinear dynamics in nuclear and other finite systems, Beijing 2001, edited by Z.Li, K. Wu, X. Wu, E. Zhao and F. Sakata ( American Institute of Physics) P. 209.
- [6] M. Trotta, A. M. Stefanini, L. Corradi and et. al., Phys. Rev. **C 65**, 011601 (R) (2001).
- [7] H.Timmers, D.Ackermann, S.Beghini, L.Corradi, J.H.He, G.Montagnoli, F.Scarlassara, A.M.Stefanini, N.Rowley, Nucl. Phys. **A633**, 421 (1998).
- [8] Yu. Oganessian, et. al., Phys. Rev. **63**, 011301 (R) (2001).
- [9] M.Beckerman, Phys. Rep. **129**,145 (1985); Rep. Prog. Phys. **51**, 1047 (1988).
- [10] R.Vandenbosch, Annu. Rev. Nucl. Part. Sci. **44**, 447 (1992).
- [11] W.Reisdorf, J. Phys. **G20**, 1297 (1994).
- [12] A.B.Balantekin and N.Takigawa, Rev. Mod. Phys. **70**, 77 (1998).
- [13] Proceedings of the International Workshop on "Heavy Ion Collisions at Near Barrier Energies", J. Phys. **G23**,1157 (1997).

[14] K.Hagino, N.Takigawa, M.Dasgupta, D.J.Hinde, and J.R.Leigh, Phys. Rev. Lett. **79**, 2014 (1997); K.Hagino, N.Takigawa, and S.Kuyucak, *ibid.* **79**, 2943 (1997).

[15] V.N.Kondratyev, A.Bonasera, and A.Iwamoto, Phys. Rev. **C61**, 044613 (2000).

[16] Ning Wang, Zhuxia Li, Xizhen Wu, Phys. Rev. **C 65**, 064608 (2002).

[17] Ch.Hartnack, Zhuxia Li, L.Neise, G.Peilert, A.Rosenhauser, H.Sorge, J.Aichelin, H.Stoecker and W.Greiner, Nucl. Phys. **A495**, 303 (1989);  
Zhuxia Li, Ch.Hartnack, H.Stoecker and W.Greiner, Phys. Rev. **C 40**, 824 (1991).

[18] J.Aichelin, Phys. Rep. **202** 233 (1991), and references therein.

[19] Ch.Hartnack, Rajeev K.Puri, J.Aichelin, Eur. Phys. J. **A1**, 151 (1998).

[20] A.Ono, H.Horiuchi, Toshiki Maruyama, and A.Ohnishi, Phys. Rev. Lett. **68**, 2898 (1992); Y.Kanada-En'yo and H.Horiuchi, Phys. Rev. **C52**,647 (1995); Y.Kanada-En'yo, H.Horiuchi, and A. Doté, Phys. Rev. **C60**, 064304 (1999).

[21] H.Feldmeier, J.Schnack, Rev.Mod. Phys.**72**,655(2000).

[22] H.Feldmeier, J.Schnack, Prog. Part. Nucl. Phys. **39**, 392 (1997) and references therein.

[23] David H.Boal, James N.Glosli, Phys. Rev. **C37**, 91 (1988), and **C38**, 2621 (1988).

[24] D.Vautherin, D.M.Brink, Phys. Rev. **C5**,626 (1972).

[25] P. Möller, J.R. Nix, W.D. Myers and W.J. Swiateski, Atomic Data and Nuclear Data **59**,185(1995).

[26] Massimo Papa, Toshiki Maruyama, and Aldo Bonasera, Phys. Rev. **C 64**, 024612 (2001).

[27] Qingfeng Li, Zhuxia Li, Phys. Rev. **C64**, 064612 (2001).

[28] I.Hamamoto, H.Sagawa, X.Z.Zhang, Phys.Rev.**C53**,765 (1996).

[29] I.Hamamoto, H.Sagawa, X.Z.Zhang, Nucl.Phys.**648**,203. (1999).

[30] M.A.Preston and R.K.Bhaduri, Structure of the Nucleus, Addison-Wesley Publishing Co., Inc., Reading, Mass. (1975) P.10-14.

[31] T.Maruyama, K.Niita, et al. Phys. Rev, **C57**, 655 (1998).

## CAPTIONS

**Fig.1** The fusion path for a typical event of head on reaction of  $^{40}\text{Ca}+^{90}\text{Zr}$  at the energy 5 MeV below the Coulomb barrier. The thick curve is the dynamical barrier as a function of the distance between the centers of mass of projectile and target. Sub-figures (1a), (2a), (3a) are for contour plots of the density distributions of the reaction systems at the corresponding time pointed in the curve of  $V_b \sim d$ , and (1b), (2b), (3b) are the corresponding single-particle potentials at the same time as Sub-figures (1a), (2a), (3a).

**Fig.2** The fusion cross sections for  $^{40,48}\text{Ca}+^{90,96}\text{Zr}$ . The experimental data are taken from [7].

**Fig.3** The distributions of the fusion probability for reactions of  $^{40,48}\text{Ca}+^{90,96}\text{Zr}$  with respect to impact parameters.

**Fig.4** The dynamic barriers as a function of the distance of centers of mass projectile and target for head on collisions of  $^{40,48}\text{Ca}+^{90,96}\text{Zr}$  at the incident energy of 5 MeV below the static Coulomb barrier.

**Fig.5** The definition of the geometric quantities in Table III.

**Fig.6** The density dependence of the chemical potential of protons and neutrons for neutron rich systems.

**Fig.7** The time evolution of the N/Z ratio at the neck region for fusion reactions of  $^{40,48}\text{Ca}+^{90,96}\text{Zr}$ . The right panel is for the case at the energy of 10 MeV above the static Coulomb barrier and the left panel is for the case at the energy of 5 MeV below the static Coulomb barrier.

**Table.1** The parameters used in the calculations.

**Table. 2** The comparison between the static Coulomb barrier and the dynamic barrier for reactions of  $^{40,48}\text{Ca}+^{90,96}\text{Zr}$ .

**Table.3** The quantities relevant to the dynamic barrier calculated at the time when the dynamic barrier reaches the highest value in the fusion path.

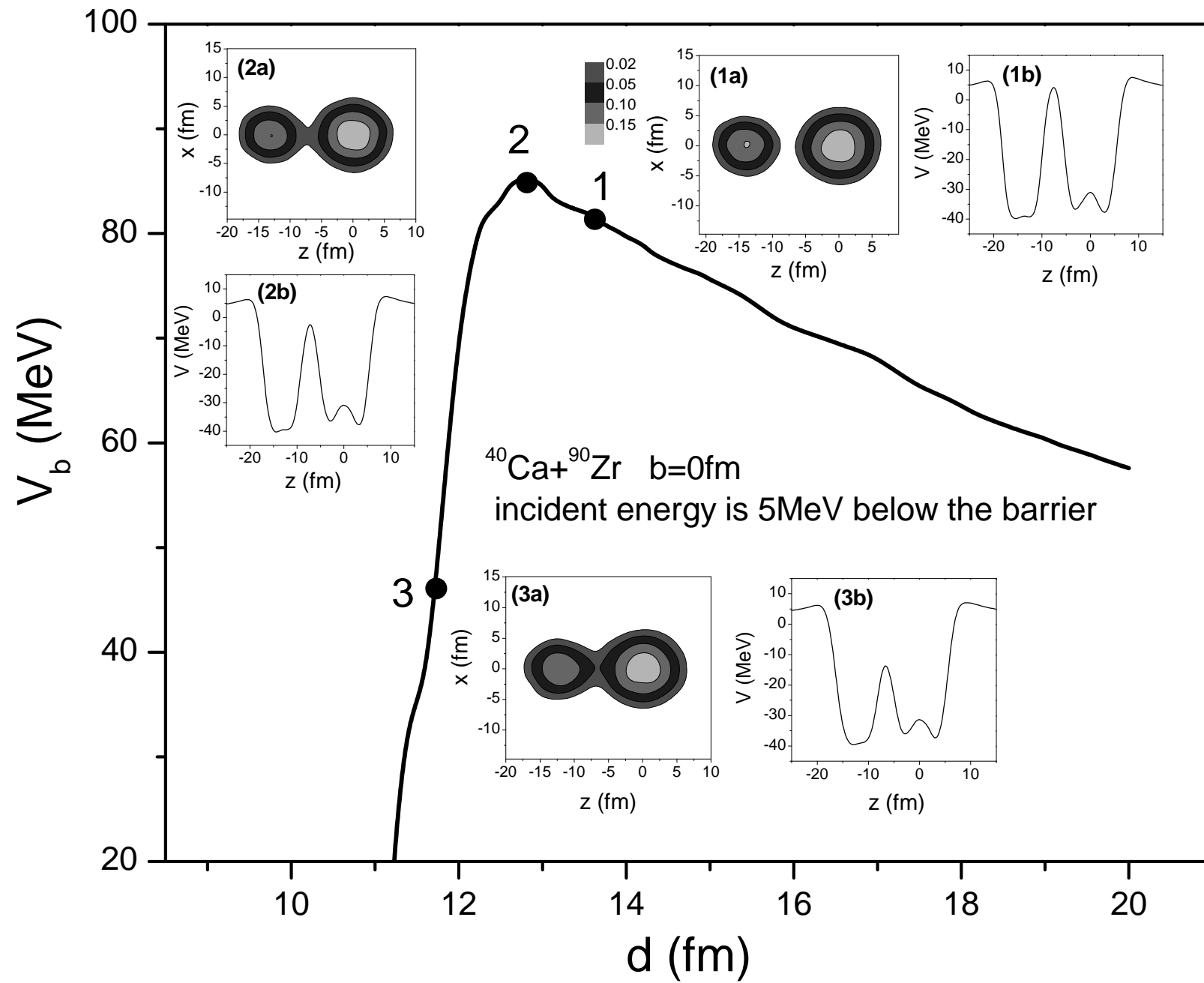


**Table.1**

$\alpha(GeV)$	$\beta(GeV)$	$\rho_0(fm^{-3})$	$g_0(GeVfm^5)$	$C_s(GeV)$	$C_k(fm^5)$
-0.124	0.071	0.165	0.96	0.032	1.0

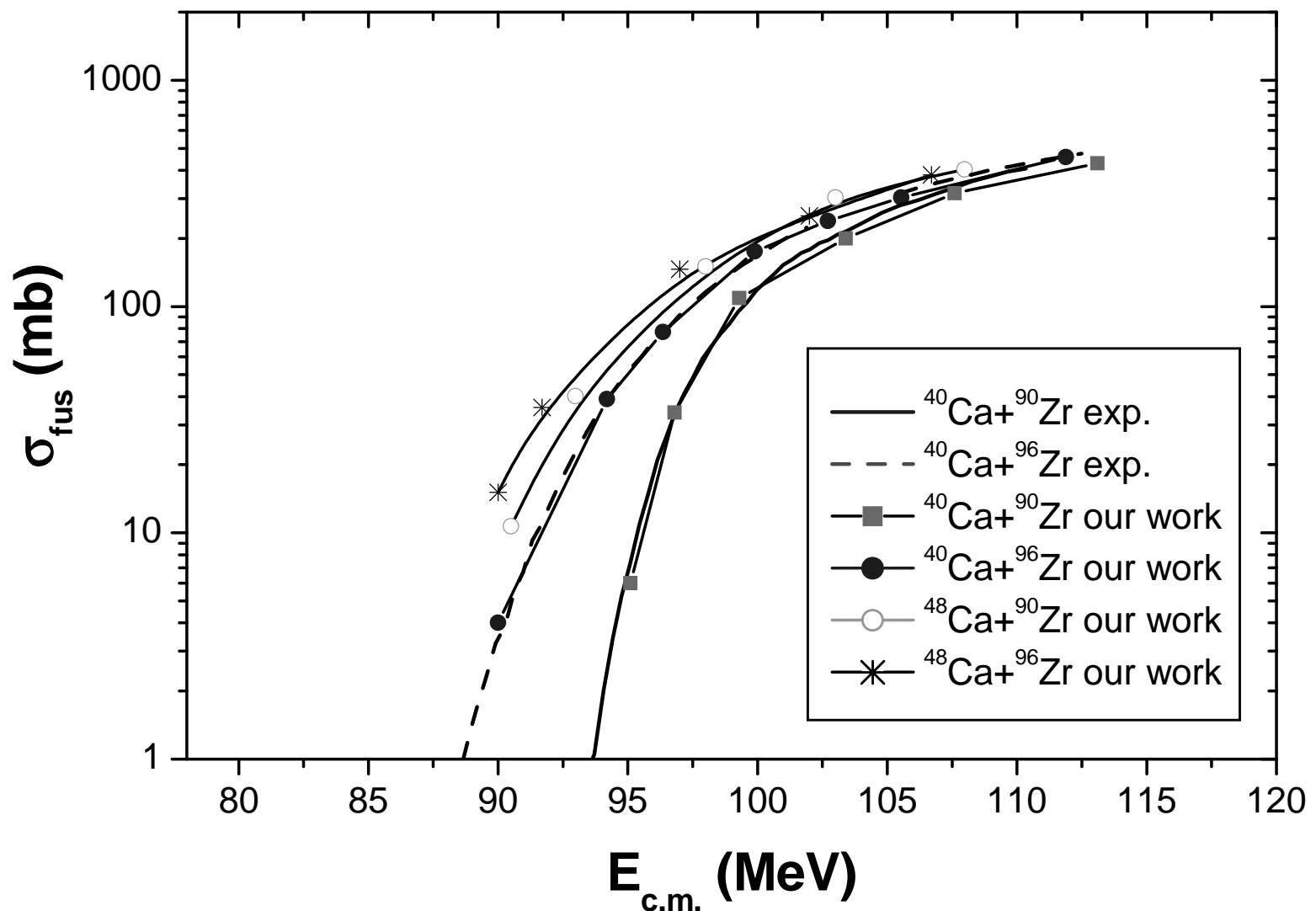


Table.2

Reaction	$^{40}\text{Ca} + ^{90}\text{Zr}$		$^{40}\text{Ca} + ^{96}\text{Zr}$		$^{48}\text{Ca} + ^{90}\text{Zr}$		$^{48}\text{Ca} + ^{96}\text{Zr}$	
$E_{\text{c.m.}}(\text{MeV})$	93.8	108.8	92.3	107.3	92.5	107.5	92.1	107.1
Time reaching the top of barrier (fm/c)	171	141	172	142	176	146	177	145
Height of dynamic barrier (MeV)	85.7	88.6	83.8	87.5	84.3	87.2	84.0	86.5
Dynamic lowering (MeV)	13.1	10.2	13.5	9.8	13.2	10.3	13.1	10.6
Height of static barrier (MeV)	98.8		97.3		97.5		97.1	

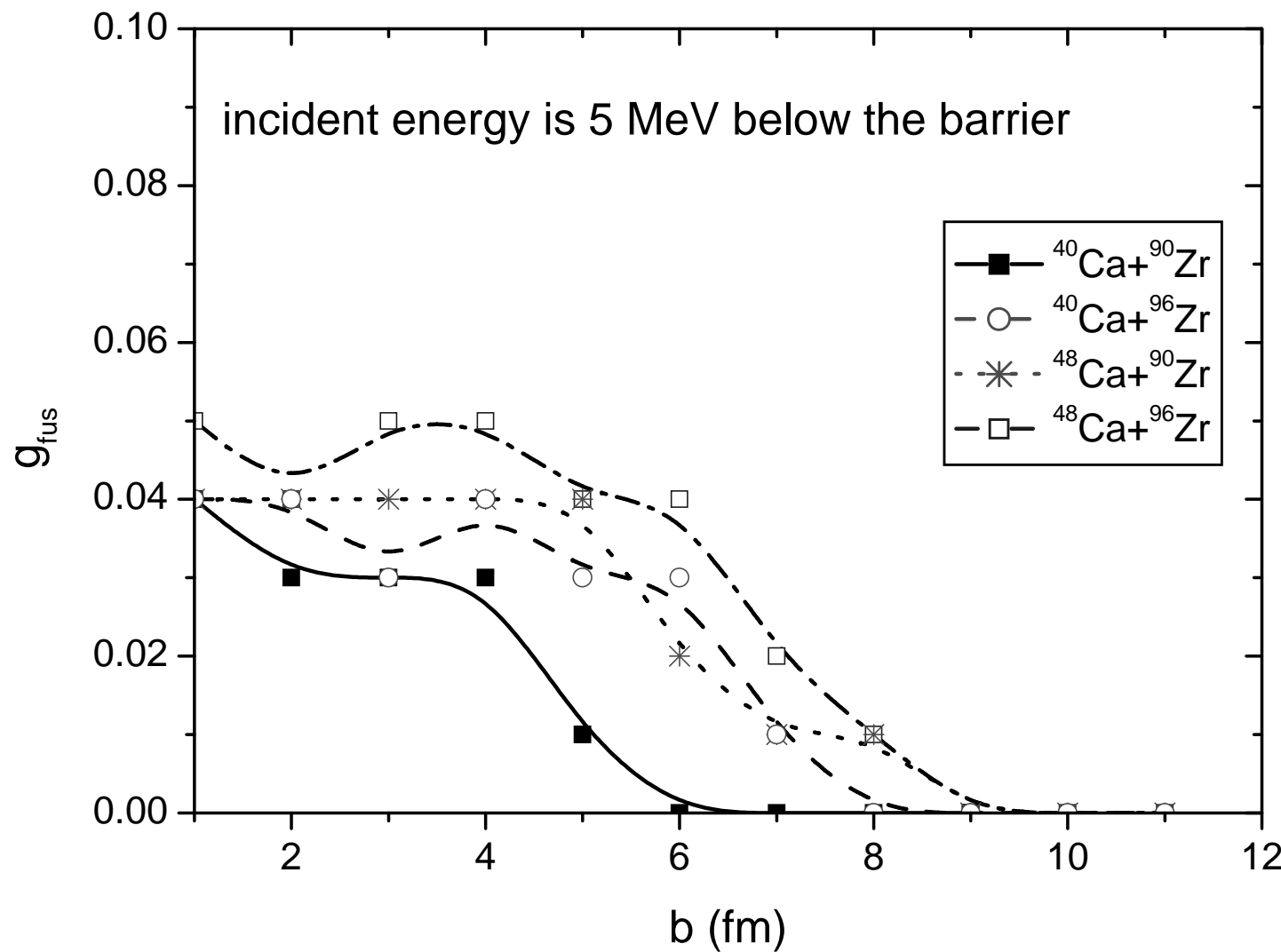


Table.3

Reaction	$^{40}\text{Ca} + ^{90}\text{Zr}$		$^{40}\text{Ca} + ^{96}\text{Zr}$		$^{48}\text{Ca} + ^{90}\text{Zr}$		$^{48}\text{Ca} + ^{96}\text{Zr}$	
$E_{\text{c.m.}}(\text{MeV})$	93.8	108.8	92.3	107.3	92.5	107.5	92.1	107.1
Height of dynamic barrier (MeV)	85.7	88.6	83.8	87.5	84.3	87.2	84.0	86.5
Distance between centers of mass $\mathbf{d}$ (fm)	13.01	12.50	13.24	12.72	13.26	12.78	13.40	12.96
Elongation (fm)	5.23	4.72	5.35	4.83	5.31	4.83	5.34	4.90
N/Z at neck region	1.210	1.165	1.407	1.323	1.468	1.360	1.610	1.577
Width of neck $\Delta$ (fm)	1.92	2.22	1.89	2.15	1.91	2.20	1.95	2.16
$\rho$ at neck (fm $^{-3}$ )	0.027	0.029	0.027	0.028	0.027	0.029	0.027	0.027
N/Z of total system	1.167		1.267		1.300		1.400	

